Rate Coefficients and Equilibrium Constant for the $CH_2CHO + O_2$ Reaction System†

Eric Delbos,[⊥] Christa Fittschen,*[,⊥] Horst Hippler,[‡] Nikolina Krasteva,[‡] Matthias Olzmann,*[,‡] and Bela Viskolcz[§]

Physicochimie des Processus de Combustion et de l'Atmosphere UMR CNRS 8522 and Centré d'Etudes et Recherches Lasers et Applications, Université des Sciences et Technologies de Lille 1, 59655 Villeneuve d'Ascq Cedex, France, Institut für Physikalische Chemie, Universität Karlsruhe (TH), Kaiserstrasse 12, D-76128 Karlsruhe, Germany, and Department of Chemistry, Juhász Gyula Teachers' Training College, University of Szeged, H-6701 Szeged, P. O. Box 396, Hungary

Received: August 19, 2005; In Final Form: October 16, 2005

The kinetics of the $CH_2CHO + O_2$ reaction was experimentally studied in two quasi-static reactors and a discharge flow-reactor at temperatures ranging from 298 to 660 K and pressures between 1 mbar and 46 bar with helium as the bath gas. The CH_2CHO radicals were produced by the laser-flash photolysis of ethyl vinyl ether at 193 nm and by the reaction $F + CH_3CHO$, respectively. Laser-induced fluorescence excited at 337 or 347.4 nm was used to monitor the CH_2CHO concentration. The reaction proceeded via reversible complex formation with subsequent isomerization and fast decomposition: $CH_2CHO + O_2 \leftrightarrow O_2CH_2CHO \rightarrow HO_2$-$CH_2CO \rightarrow$ products. The rate coefficients for the first and second steps were determined (k_1, k_{-1}, k_2) and analyzed by a master equation with specific rate coefficients from the Rice−Ramsperger−Kassel−Marcus (RRKM) theory. Molecular and transition-state parameters were obtained from quantum chemical calculations. A third-law analysis led to the following thermodynamic parameters for the first step: $\Delta_R S°_{300K(1)} = -144$ J K^{-1} mol^{-1} (1 bar) and $\Delta_R H°_{300K(1)} = (-101 \pm 4)$ kJ mol^{-1}. From the falloff analysis, the following temperature dependencies for the low- and high-pressure limiting rate coefficients were obtained: $k_{1(0)} = 5.14 \times 10^{-14}$ exp(210 K/T) cm^{-3} s^{-1}; $k_{1(\infty)} = 1.7 \times 10^{-12}$ exp(−520 K/T) cm^{-3} s^{-1}; and $k_{2(\infty)} = 1.3 \times 10^{12}$ exp[−(82 ± 4) kJ mol^{-1}/RT] s^{-1}. Readily applicable analytical representations for the pressure and temperature dependence of k_1 were derived to be used in kinetic modeling.

1. Introduction

Vinoxy-type radicals, R_1CHCR_2O, occur as intermediates in the ozonolysis of alkenes,[1] which is a significant degradation path for unsaturated hydrocarbons in the atmosphere. Here, the vinoxy radical itself (CH_2CHO) is formed from olefines of the type $CH_3CH{=}CR_1R_2$.[2,3] Moreover, CH_2CHO formation was observed in reactions such as $O + C_2H_4$,[4−7] $O + C_2H_3$,[8] and $OH + C_2H_2$,[9] all of which are important in hydrocarbon combustion. Also, a recent modeling study showed that CH_2-CHO occurs in substantial amounts during the ignition of ethanol.[10]

In the presence of O_2, vinoxy is mainly consumed by the reaction sequence

$$CH_2CHO + O_2 \leftrightarrow O_2CH_2CHO \quad (1)$$

$$O_2CH_2CHO \rightarrow \text{products} \quad (2)$$

which is a part of large scale combustion mechanisms.[11] The kinetics of the $CH_2CHO + O_2$ reaction has been investigated by several groups, but the experiments were mostly restricted to room temperature. In an early work, Gutman and Nelson[12] studied reaction 1 in a quasi-static flow-reactor. Vinoxy radicals were generated by the laser-flash photolysis of methyl vinyl ether and monitored by laser-induced fluorescence (LIF) under pseudo-first-order conditions with respect to O_2. Rate coefficients as a function of temperature (295 K ≤ T ≤ 476 K) and pressure (2 mbar ≤ P ≤ 133 mbar, buffer gases: N_2, SF_6) were determined, where a slightly negative temperature dependence and a weak positive pressure dependence was observed. These results were interpreted by assuming reaction 1 to be an association step near the high-pressure limit. The authors also discussed the possibility of a consecutive 1,4 hydrogen migration in the adduct followed by a fast decomposition toward $CH_2O + CO + OH$. In a similar experimental approach, Lorenz et al.[13] studied reaction 1 at 298 K and pressures between 10 and 280 mbar (helium). From a falloff analysis, a high-pressure limiting rate coefficient $k_{1(\infty)} = (2.6 \pm 1.5) \times 10^{-13}$ cm^3 s^{-1} was obtained, and the temperature dependence near 300 K at gas densities of 1×10^{18} cm^{-3} was given as $k_1 = (2.7 \pm 1.5) \times 10^{-14}$ exp(668 K/T) cm^3 s^{-1}. Moreover, OH radicals were identified as a reaction product with a yield of 20% at 27 mbar. Zhu and Johnston[14] monitored the disappearance of CH_2CHO caused by reaction 1, using cavity ring-down spectrometry at T = 298 K in a pressure range from 3 to 540 mbar with N_2 as bath gas. These authors obtained rate coefficients slightly below those of the earlier works, and a falloff analysis gave $k_{1(\infty)} = (1.9 \pm 0.2) \times 10^{-13}$ cm^3 s^{-1}. Glyoxal was found as a reaction product but was assigned to secondary reactions. Finally, in a very recent study, Oguchi et al.[15] determined rate coefficients and relative OH yields for reaction 1 using LIF. The experiments were performed at room temperature and pressures between 4

† Part of the special issue "Jürgen Troe Festschrift".

* Corresponding authors. E-mail: christa.fittschen@univ-lille1.fr (C.F.); olzmann@chemie.uni-karlsruhe.de (M.O.).

⊥ CNRS Lille.

‡ Universität Karlsruhe (TH).

§ University of Szeged.

10.1021/jp054697s CCC: $33.50
Published on Web 12/02/2005

and 270 mbar (helium). The pressure-dependent rate coefficients obtained are in good agreement with the earlier values of Nelson and Gutman, and OH was found to be a direct product with yields decreasing from ~20% at 12 mbar to ~10% near 270 mbar (tentative results).[16]

In all these studies, reaction 1 was found to be comparatively slow with a slightly pressure-dependent rate coefficient ranging from 1×10^{-13} cm^3 s^{-1} near 1 mbar to $\sim 2 \times 10^{-13}$ cm^3 s^{-1} above 100 mbar for $T \approx 300$ K. In the only temperature-dependent study, Gutman and Nelson[12] observed a weak negative temperature dependence in the above pressure range.

Recent theoretical studies[17−19] essentially confirmed the mechanism proposed in these experimental works. It was shown that reactions 1 and 2 are likely to proceed via chemically activated intermediates (in the following, labeled by *) with subsequent isomerization-dissociation steps in competition to collisional stabilization (bath gas M):

$$CH_2CHO + O_2 \leftrightarrow O_2CH_2CHO^* \qquad (1a, -1a)$$

$$O_2CH_2CHO^* + M \rightarrow O_2CH_2CHO + M \qquad (1b)$$

$$O_2CH_2CHO^* \rightarrow HO_2CH_2CO^* \qquad (2a)$$

$$HO_2CH_2CO^* \rightarrow HO_2CH_2^* + CO \qquad (3)$$

$$HO_2CH_2^* \rightarrow OH + CH_2O \qquad (4)$$

Lee and Bozzelli[17] calculated molecular and thermochemical data for this reaction sequence by different quantum chemical methods and predicted rate coefficients and product yields using a quantum Rice−Ramsperger−Kassel (QRRK)/master equation approach. These authors showed that reactions 3 and 4 are much faster than reaction −2a (the inverse of reaction 2a) and also faster than collisional stabilization. Therefore, reaction 2a can be written as being irreversible, and the collisional deactivation steps for $HO_2CH_2CO^*$ and $HO_2CH_2^*$ need not to be included in the above scheme. Additional reactions with higher activation barriers exist but were shown to be negligible at temperatures below 1000 K and pressures above 10 mbar. Similar thermochemical data were obtained in three more quantum chemical studies by Kuwata et al.[18,19] and Oguchi et al.[20] Apart from the latter work, however, no attempts have been made to relate the predicted molecular parameters to experimental results. Only Oguchi et al.[20] fitted a falloff curve for reaction 1 to the results of ref 14 and obtained a comparatively large high-pressure limiting rate coefficient $k_{1(\infty)} = 1.3 \times 10^{-12}$ cm^3 s^{-1} ($T = 298$ K).

To better characterize the kinetics and the mechanism of the $CH_2CHO + O_2$ reaction, we performed the first experiments over an extended temperature and pressure range (298 K < T < 660 K; 10^{-3} bar < P < 50 bar) and analyzed our results in terms of statistical rate theory with molecular parameters from quantum chemical calculations. From this combined experimental and theoretical study, we derive thermodynamic and kinetic parameters, which can be used in atmospheric and combustion modeling.

2. Experimental Section

The experiments were essentially carried out in 2 different quasi-static reactors, one suited for pressures between 40 mbar and 5 bar located at the CNRS Lille,[21] and the other one designed for pressures from 1 to 1000 bar located at the University of Karlsruhe.[22,23] A few supplementary measurements at room temperature below 15 mbar were performed in a discharge flow-reactor also located in Lille.[21] Because both of the experimental setups have been described in detail elsewhere,[21−23] only the essentials are repeated here.

The reaction cells (in the order Lille/Karlsruhe) are made of stainless steel and can be heated to 600/1000 K, where the temperature is controlled by 1/2 thermocouple/s placed directly within the reaction zone/at the entrance and exit of the gas flow. Vinoxy radicals are generated by excimer laser photolysis of ethyl vinyl ether at 193 nm (Lambda Physik LPX 202i/Compex 102). The precursor concentrations were in the range $(1-2) \times 10^{11}/(2-10) \times 10^{14}$ cm^{-3}. By adopting the absorption cross-section of methyl vinyl ether, $\sigma_{193\ nm} = 8 \times 10^{-18}$ cm,[2,24] and using an average photolysis-laser fluence of 30/(1−15) mJ cm^{-2} and a quantum yield of unity, we estimate the initial vinoxy radical concentrations to be in the range $(2-4) \times 10^{10}/(3-20) \times 10^{11}$ cm^{-3}. At such low concentrations and under pseudo-first-order conditions with respect to O_2 (5×10^{15} cm$^{-3} \leq [O_2] \leq 3 \times 10^{17}$ cm^{-3}), unwanted reactions are effectively suppressed. This was carefully checked by varying the precursor concentration, the laser fluence, and the oxygen concentration.

The progress of reaction 1 was followed by recording the LIF of CH_2CHO after excitation at 347.4 nm/337 nm (for a fluorescence excitation spectrum, see ref 4). The probe beam came from a frequency-doubled dye laser (Quantel TDL 50 with DCM/LDS 698 for Vinoxy and Rhodamin 590 for OH, 0.6 × 0.4 cm^2, 5 mJ per pulse/Lambda Physik Scanmate 2E with p-Terphenyl, 0.2 × 0.2 cm^2, 3 mJ per pulse) pumped by a frequency-doubled YAG laser (Quantel YG 781C)/excimer laser (Lambda Physik Compex 102, XeCl). The photolysis and probe beam propagated antiparallel through the cell, and the fluorescence was collected perpendicular to the beams by a photomultiplier (Hamamatsu R 212) after passing through a cutoff filter (λ > 375 nm)/monochromator (Zeiss M4 QIII centered at 400 ± 20 nm). The signal from the photomultiplier was amplified (Stanford Research Systems SR240), boxcar integrated (EG&G 4121B/Stanford Research Systems SR250), digitized (Stanford Research Systems SR245), and further processed on a personal computer. Typical decay curves consisted of fluorescence intensities at 30/50−100 different delay times; each averaged over 50−100/8−10 laser shots (repetition rate: 2−10 Hz).

In Lille the reaction mixtures, ethyl vinyl ether + He and O_2 + He, respectively, were prepared and separately stored. Low flows (1−10 standard temperature and pressure (STP) cm^3 min^{-1}) of these mixtures were then passed through calibrated flow controllers (Tylan FC-260) and admixed to the main flow of helium (100−1000 STP cm^3 min^{-1}). The total flow rate was adapted to obtain a flow velocity of about 1 cm s^{-1} within the reaction cell (perpendicular to the laser beam) so as to prevent the accumulation of reaction products. Experiments at total pressures between 40 mbar and 5 bar at temperatures ranging from 298 to 500 K have been performed with this setup.

In Karlsruhe, reaction mixtures consisting of ethyl vinyl ether, O_2, and He were prepared and stored under high pressure in commercially available gas cylinders (Messer Griesheim, 40 dm^3, 300 bar). They were allowed to homogenize for at least 12 h before use. The flow through the reaction cell was regulated by a flow controller (Bronkhorst, F-231M-FAC-33-P) and kept between 2 and 5 STP dm^3 min^{-1} so as to avoid the enrichment of photolysis and reaction products in the reactor. With this setup, experiments at pressures between 2 and 50 bar in the temperature range 298−660 K were performed. In either of our quasi-static setups (Lille and Karlsruhe), the uncertainty in the temperature is estimated to be ± 3 K.

The experiments in the discharge flow-reactor at room temperature have been conducted and analyzed in exactly the same way as that described in ref 21 for the $CH_2CHO + NO$ reaction. In brief, vinoxy radicals were generated by the reaction $F + CH_3CHO$ and admixed to the main gas flow containing O_2 and He (F atoms from a microwave discharge burning in a CF_4/He mixture). The rate coefficients k_1 were obtained by measuring the fluorescence intensity of CH_2CHO at different distances downstream the admixture point for varying O_2 concentrations. Simple corrections for the pressure drop and diffusion effects were applied.[21]

The following gases and chemicals were used: helium (Air Liquide, 99.995%/Messer Griesheim, 99.999%), O_2 (Air Liquide, 99.9%/Messer Griesheim, 99.995%), ethyl vinyl ether (Fluka, 99%/Merck, 99%; degassed before use), CH_3CHO (99.5% Acros Organics), and CF_4 (98% Air Liquide).

The detailed experimental conditions and the primary results can be found in Tables IS and IIS of the Supporting Information.

3. Calculations

To analyze our experimental results in terms of statistical rate theory, we performed quantum chemical calculations for the stable species and the transition states of the above mechanism. Rotational constants and harmonic frequencies were obtained from Møller−Plesset perturbation theory at the MP2/6-311G(d,p) level,[25,26] and single-point energies were calculated with the following methods (energy//optimized geometry): (1) QCISD(T)/6-311+G(3df,2p)//QCISD/6-311G(d,p), (2) CCSD(T)/cc-pVTZ//QCISD/6-311G(d,p), and (3) B3LYP/6-311+G(3df,2p)//B3LYP/6-311G(d,p). Here, QCISD(T) and CCSD(T) denote quadratic configuration interaction[27] and coupled cluster[28,29] calculations, respectively, with single and double excitations including triples corrections.[27] B3LYP stands for the density functional theory (DFT)[30] employing the Becke-3−Lee−Yang−Parr functional.[31] The well-known Gaussian triple-ζ basis sets[26] and Dunning's correlation consistent basis set (cc-pVTZ),[32] respectively, were used. The computations were performed with the Gaussian 98 program package.[33]

From the results of these quantum chemical calculations, temperature and pressure-dependent rate coefficients $k_1(T,P)$ were calculated from statistical rate theory. Under steady-state conditions and based on the above mechanism, $k_1(T,P)$ can be written as the product of the high-pressure limiting rate coefficient $k_{1(\infty)}(T)$ and a pressure-dependent yield factor:[34]

$$k_1(T,P) = k_{1(\infty)}(T)\frac{D_{2a}(T,P) + S(T,P)}{D_{-1a}(T,P) + D_{2a}(T,P) + S(T,P)} \quad (5)$$

Here, $D_i(T,P)$ is the rate of reaction for the unimolecular step i, and $S(T,P)$ is the rate of collisional stabilization of $O_2CH_2CHO^*$ (eq 1b). The rates of the unimolecular reactions can be expressed as[35]

$$D_i(T,P) = \int_0^\infty k_i(E)n(E;T,P)\mathrm{d}E \quad (6)$$

with the specific rate coefficients $k_i(E)$ and the energy-dependent O_2CH_2CHO population $n(E;T,P)$. In our calculations, we obtained the specific rate coefficients from the Rice−Ramsperger−Kassel−Marcus (RRKM) theory:[35−37]

$$k_i(E) = \frac{W_i(E - E_{0(i)})}{h\rho(E)} \quad (7)$$

where $W_i(E)$ denotes the sum of states of the transition state for reaction i, $E_{0(i)}$ is the corresponding threshold energy, h is Planck's constant, and $\rho(E)$ is the density of states of O_2CH_2CHO. The population $n(E;T,P)$ is obtained by solving the steady-state master equation[35,36]

$$R_{1a}f(E) - \omega n(E) + \omega\int_0^\infty P(E,\epsilon)n(\epsilon)\mathrm{d}\epsilon - [k_{-1a}(E) + k_{2a}(E)]n(E) = 0 \quad (8)$$

for given values of T and P. Here, R_{1a} is the rate of formation of the chemically activated $O_2CH_2CHO^*$ radicals, $f(E)$ is their nascent distribution function, ω is the Lennard−Jones collision frequency, and $P(E,\epsilon)$ the probability density for a collision-induced transition $E \leftarrow \epsilon$. The distribution function $f(E)$ is calculated from the relation[35,36]

$$f(E) = \frac{W_{1a}(E - E_{0(-1a)})\exp[-(E - E_{0(-1a)})/RT]}{\int_0^\infty W_{1a}(\epsilon)\exp(-\epsilon/RT)\mathrm{d}\epsilon} \quad (9)$$

and a stepladder model obeying detailed balancing is used for the transition probabilities.[35,36] The step size ΔE_{SL} (corresponding to the average energy transferred per down collision) was treated as an adjustable parameter. All densities and sums of states were determined by direct counting procedures[38−40] in the rigid rotor harmonic oscillator approximation for a total angular momentum quantum number $J = 44$, which is the average J for O_2CH_2CHO at $T = 300$ K. We adopted this value also for all other temperatures, because the influence of varying J is small due to the tight transition states in our system.[35,36] Equation 8 is set up in discrete form with a grain size of 10 cm^{-1} and solved by standard routines for tridiagonal matrixes.[41] For the calculation of the yield factor in eq 5, only the ratios D_{-1a}/R_{1a}, D_{2a}/R_{1a}, and S/R_{1a} are required because R_{1a} cancels. Hence, eq 8 can be divided by R_{1a}, and the solution yields $n(E;T,P)/R_{1a}$. Substitution of this quantity into eq 6 results in relative unimolecular rates D_i/R_{1a}, and one obtains the relative rate of collisional stabilization from the steady-state condition $S/R_{1a} = 1 - D_{-1a}/R_{1a} - D_{2a}/R_{1a}$. Energy zero is the rovibrational ground state of O_2CH_2CHO. More technical details of our master equation can be found in ref 42.

4. Results and Discussion

Experiment. Relative concentration−time profiles for vinoxy radicals under pseudo-first-order conditions with respect to O_2 were recorded. Depending on the temperature, different temporal behavior was observed. At temperatures below 420 K, the decay curves were generally monoexponential. They became biexponential at temperatures between 420 and 500 K (depending on the O_2 concentration and the time scale of the experiment) and again monoexponential at temperatures above 570 K. This can be explained by the increasingly rapid equilibration of reaction 1 with increasing temperature.

At temperatures below 420 K, the reverse reaction of eq 1 is too slow, and the monoexponential decay is governed by the rate coefficient k_1. The concentration−time profiles were analyzed in terms of the pseudo-first-order rate law $\ln([CH_2CHO]/[CH_2CHO]_0) = -(k_1[O_2] + k_d)t \equiv k_{obs}t$. Here, the correction term k_d essentially accounts for reactions of CH_2CHO with the precursor and with impurities as well as for the wall loss in the discharge flow-apparatus and the diffusion out of the observation volume in the flash-photolysis setup, respectively. The rate coefficient k_1 was obtained by plotting k_{obs} versus $[O_2]$. We verified that the intercept k_d was always close to the values measured in separate experiments without

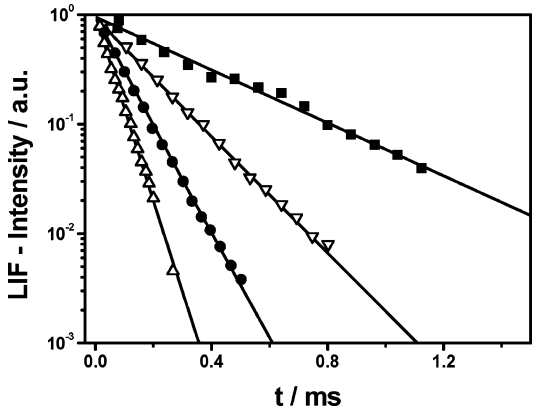

Figure 1. Logarithmic plot of the fluorescence decays and linear fits for $T = 298$ K, $P = 133$ mbar, and different O_2 concentrations ($[O_2]/10^{16}$ cm^{-3}: ■ = 1.3; ▽ = 2.8; ● = 5.1; △ = 8.7).

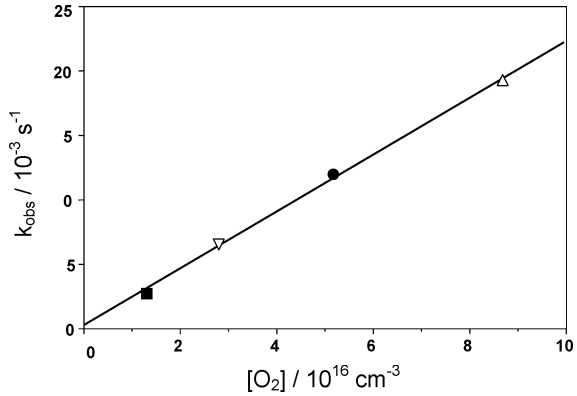

Figure 2. Plot of the observed rate coefficient vs $[O_2]$ (for conditions and symbols see Figure 1).

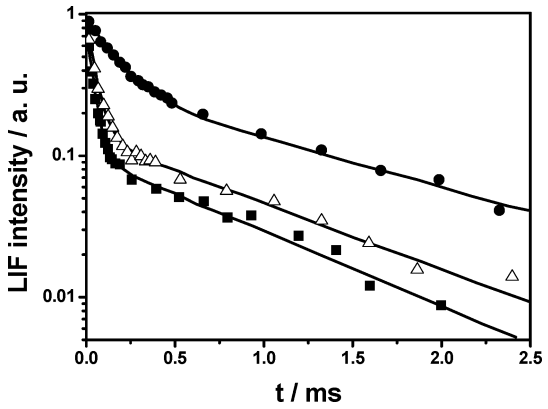

Figure 3. Fluorescence decay and nonlinear fit for $T = 459$ K, $P = 666$ mbar and different O_2 concentrations ($[O_2]/10^{16}$ cm^{-3}: ● = 2.3; △ = 6.8; ■ = 11.1).

O_2. Linearized intensity−time profiles and a corresponding plot of k_{obs} versus $[O_2]$ are shown in Figures 1 and 2, respectively. The bimolecular rate coefficients k_1 and the detailed experimental conditions are collected in Table IS of the Supporting Information. They are also displayed (and compared with modeling results) in Figure 6.

At temperatures above 420 K, the vinoxy concentration does not decay to zero, and a residual signal can be observed, which slowly decreases on a millisecond time scale. Examples for such biexponential decays are shown in Figure 3. This behavior is typical for a consecutive reaction proceeding via a preequilibrium. With increasing O_2 concentration, the equilibrium of reaction 1 is shifted to the product side, and the residual vinoxy

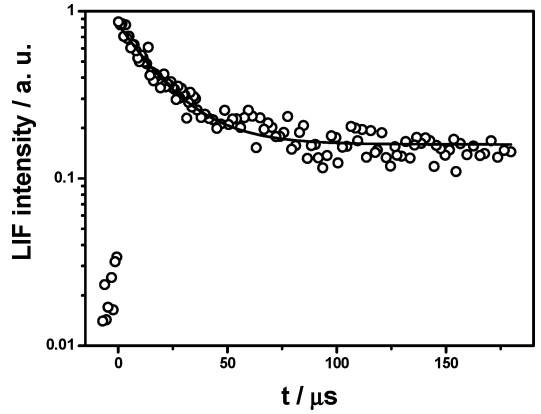

Figure 4. Fluorescence decay and equilibrium fit for $T = 516$ K, $P = 5.4$ bar, and $[O_2] = 1.2 \times 10^{17}$ cm^{-3}.

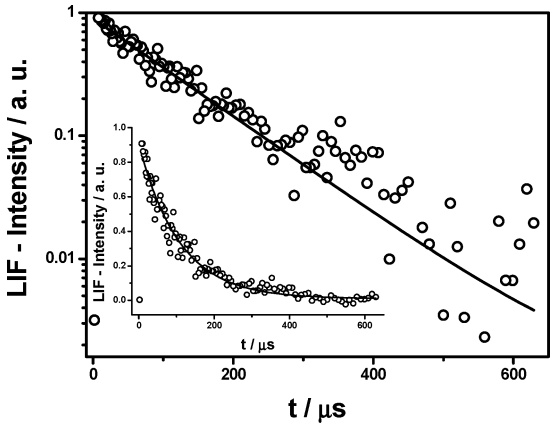

Figure 5. Fluorescence decay and linear fit for $T = 618$ K, $P = 2.6$ bar, and $[O_2] = 1.3 \times 10^{17}$ cm^{-3}.

concentration is lowered. The long-time decrease of the vinoxy concentration is assumed to be due to the consecutive reaction, eq 2, which depletes the equilibrium concentration of CH_2CHO. In the Lille group for this regime, the rate coefficients k_1, k_{-1}, and k_2 were obtained from a nonlinear least-squares fit based on the rate law for CH_2CHO in terms of reactions 1, −1, and 2. Under pseudo-first-order conditions, this rate law can be analytically integrated and analyzed in analogy to the approach in ref 43. In the Karlsruhe group, emphasis was placed on the first part of the decay curve, that is, on reaction times well below 1 ms. Therefore, the values obtained for k_2 were not significant, and, accordingly, the fluorescence-time profiles were fitted by a simpler rate law containing the opposing reactions 1 and −1 only. An example is given in Figure 4. The results are collected in Table 1 and displayed in Figures 8 and 9. More details are given in Table IIS of the Supporting Information.

For temperatures above 570 K the decays become again monoexponential; an example is shown in Figure 5. The equilibrium of reaction 1 is established rapidly on the time scale of our experiments, and reaction 2 becomes the rate-determining step. In this case, the pseudo-first-order rate coefficient can be expressed in the form $k_{obs} = k_2K_1[O_2]/(1 + K_1[O_2])$. The observed rate coefficients k_{obs} together with the experimental conditions are given in Table IIIS of the Supporting Information. The values resulting for k_2 with equilibrium constants K_1 from our third-law analysis (see below) are collected in Table 2 and displayed in Figure 9.

According to the above reaction mechanism, OH is an important product. We observed OH by LIF (excitation at 282 nm, detection at 308 ± 10 nm), and typical intensity−time

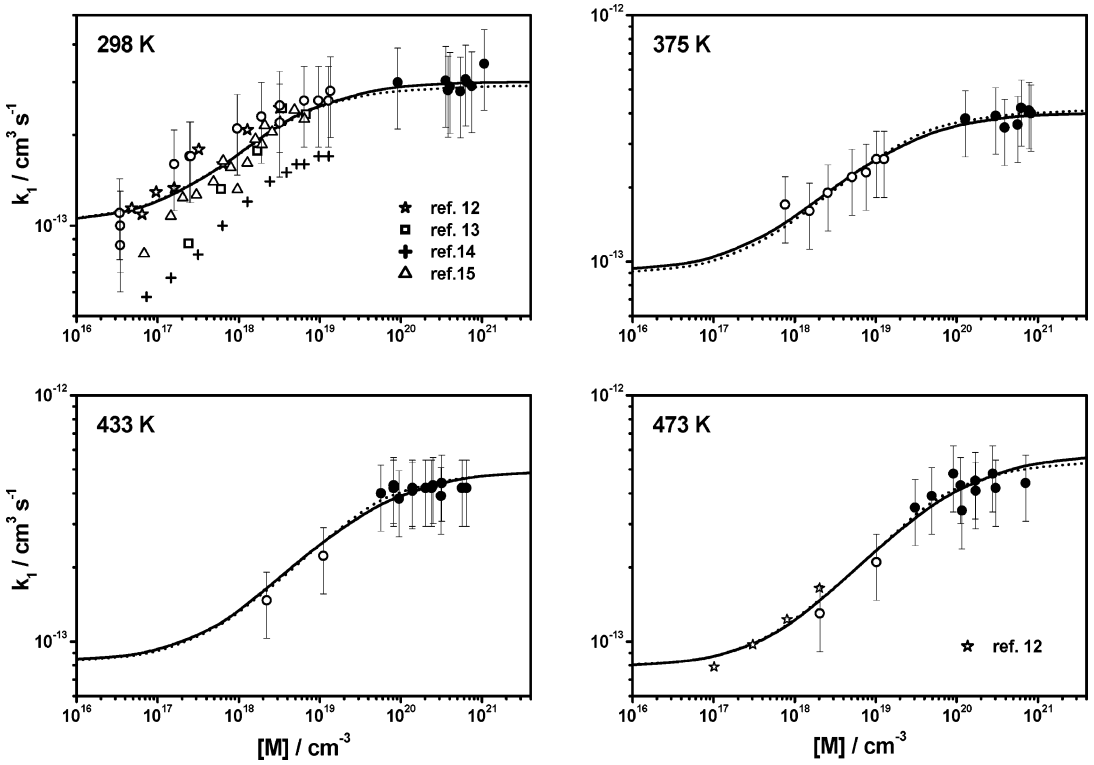

Figure 6. Pressure dependence of the rate coefficient k_1 at different temperatures: experimental results from the present work (● = Karlsruhe, ○ = Lille), previously published results,[12−15] and calculated falloff curves (solid line = master equation; dotted line = fit according to eqs 10−17).

TABLE 1: Mean Values of the Equilibrium Constant K_1 and the Rate Coefficient k_2[a]

T (K)	K_1 (cm^3)	k_2 (s^{-1})
424	(2.7 ± 0.9) E−15[b]	250 ± 90[b]
433	(1.5 ± 0.2) E−15[b]	260 ± 50[b]
445	(1.2 ± 0.3) E−15[b]	300 ± 70[b]
453	(8.4 ± 5.7) E−16[b]	490 ± 270[b]
464	(4.8 ± 3.2) E−16[b]	880 ± 310[b]
473	(1.8 ± 0.6) E−16[c]	
482	(3.0 ± 1.5) E−16[b]	1200 ± 300[b]
484	(1.2 ± 0.4) E−16[c]	
490	(9.1 ± 2.7) E−17[b]	2100 ± 500[b]
493	(8.8 ± 2.6) E−17[c]	
494	(2.4 ± 1.1) E−16[b]	1600 ± 600[b]
497	(7.5 ± 2.3) E−17[c]	
500	(6.1 ± 1.8) E−17[b]	3700 ± 300[b]
505	(4.7 ± 1.4) E−17[c]	
510	(4.7 ± 1.4) E−17[c]	
516	(3.9 ± 1.2) E−17[c]	
524	(3.2 ± 1.0) E−17[c]	
531	(2.0 ± 0.6) E−17[c]	

[a] Close-lying temperatures were lumped together; for details, see Table IIS of the Supporting Information. [b] Quasi-static reactor Lille. [c] Quasi-static reactor Karlsruhe.

profiles are shown in Figure 7. No attempts have been made to quantify the yield, but the signal intensity strongly decreased with increasing pressure. The rate coefficient of OH formation obtained from biexponential fits is in good agreement with the rate coefficient k_1 for the decay of CH_2CHO, which indicates that OH is indeed likely to be formed along the above reaction route. This is in agreement with recent finding by Oguchi et al.[15] and will be further outlined below. We note that the decreasing signal intensity in Figure 7 for increasing O_2 concentration is mainly due to fluorescence quenching.

Data Analysis. The data analysis is based on the molecular and transition-state parameters obtained from our ab initio calculations described above. The frequencies and rotational

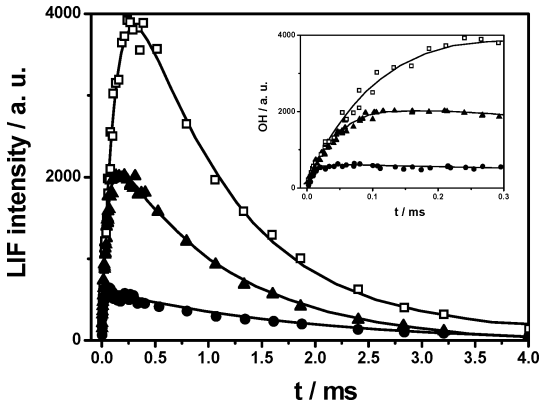

Figure 7. Fluorescence intensity of OH for different O_2 concentrations ($[O_2]/10^{16}$ cm^{-3}: □ = 2.7; ▲ = 7.0; ● = 37), T = 298 K, P = 133 mbar (He).

constants are collected in Table 3. In Figure 8, the result of a third-law analysis of the equilibrium constants K_1 is shown. The molecular data correspond to a standard entropy of reaction $\Delta_R S°_{300K(1)} = -144$ J K^{-1} mol^{-1} (1 bar), and the best fit is obtained for $\Delta_R H°_{0K(1)} = -97.0$ kJ mol^{-1}. With an error margin of ± 4 kJ mol^{-1} (see Figure 8) this corresponds to $\Delta_R H°_{300K(1)} = (-101 \pm 4)$ kJ mol^{-1}.

An Arrhenius plot for the high-pressure values of k_2 from Tables 1 (Lille) and 2 (Karlsruhe) is shown in Figure 9. The calculated molecular data correspond to $\log(A^{\infty}_2/s^{-1}) = 12.1$ at the mean temperature T = 530 K, and the best fit gives an activation energy $E^{\infty}_{a(2)} = 82.7$ kJ mol^{-1}. Again with an error margin of ± 4 kJ mol^{-1} (see Figure 9), this corresponds to a threshold energy $E_{0(2)} = (82 \pm 4)$ kJ mol^{-1}.

In view of the approximate rigid rotor/harmonic oscillator approach, we do not consider optical isomers in our third-law and transition state theory (TST) analyses.

In Figure 10, the relation of these thermochemical data to the mechanisms 1a−3 is displayed. As already noted above,

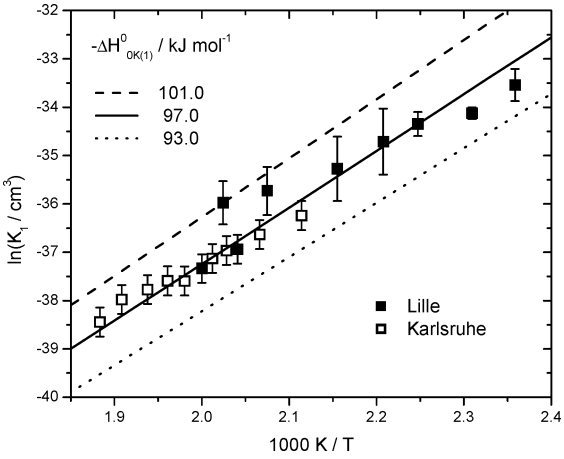

Figure 8. Temperature dependence of the equilibrium constant K_1 (from Table 1) and third-law analysis based on the calculated molecular data given in Table 3.

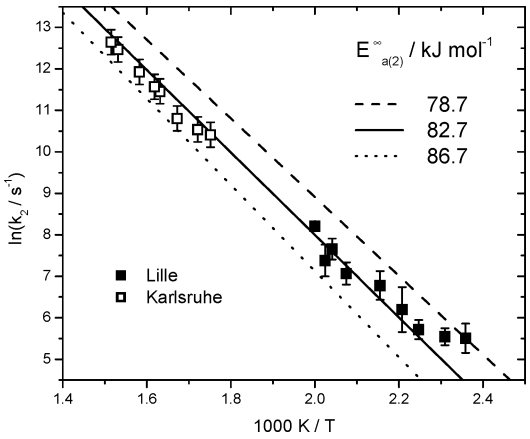

Figure 9. Temperature dependence of the rate coefficient k_2 (from Tables 1 and 2) and TST calculation based on the molecular data given in Table 3.

TABLE 2: Equilibrium Constants K_1 Calculated from Third-Law Analysis (see below) and Averaged Rate Coefficients k_2 for $T > 570$ K[a]

T (K)	K_1 (cm^3)	k_2 (10^4 s^{-1})
571	3.68 E−18	3.3 ± 1.0
581	2.59 E−18	3.8 ± 1.1
598	1.47 E−18	4.9 ± 1.5
613	9.16 E−19	9.5 ± 2.9
618	7.86 E−19	10.6 ± 3.2
632	5.20 E−19	15 ± 5
653	2.90 E−19	26 ± 8
660	2.40 E−19	31 ± 10

[a] Close-lying temperatures were lumped together; for details, see Table IIIS of the Supporting Information.

reaction 3 is much faster than reaction −2a due to its lower threshold energy and a looser transition state; $HOOCH_2$ rapidly decomposes to yield $CH_2O + OH$.[17,18] A comparison with results from quantum chemical computations is made in Table 4. It is evident that most of the quantum chemical methods predict a lower value for $-\Delta_R H°_{(1)}$ than observed. Only the values obtained at QCISD(T) and CBS level are in an order of magnitude similar to that of the experimental result. Concerning the threshold energies, DFT methods seem to underpredict $E_{0(-1)}$, whereas $E_{0(2)}$ is in a reasonable range. The highly correlated methods concordantly predict a somewhat larger barrier $E_{0(2)}$ around 96 kJ mol^{-1} and very high values for $E_{0(-1)}$. In combination with the low values for $-\Delta_R H°_{(1)}$, this leads to

TABLE 3: Vibrational Frequencies and Rotational Constants (cm^{-1}) Computed at the MP2/6-311G(d,p) Level

O_2[a]	1580, 1.446
CH_2CHO	3290, 3171, 2996, 1588, 1490, 1419, 1154, 976, 974, 702, 505, 437, 2.225, 0.3786, 0.3235
TS1	3473, 3360, 3242, 1700, 1600, 1502, 1375, 1219, 1048, 992, 719, 588, 524, 286, 149,[b]110,[b]54,[b]0.3784, 0.08429, 0.07804
O_2CH_2CHO	3200, 3126, 3000, 1790, 1471, 1423, 1359, 1284, 1248, 1116, 1058, 996, 746, 596, 445, 302, 140, 47, 0.5708, 0.09811, 0.08908
TS2	3211, 3098, 1994, 1931, 1490, 1277, 1257, 1225, 1149, 1062, 889, 742, 714, 531, 440, 401, 203, 0.5413, 0.1204, 0.1006

[a] Experimental values from Herzberg, G. *Molecular Spectra and Molecular Structure, I. Spectra of Diatomic Molecules*, 2nd ed.; Krieger: Malabar, FL, 1989. [b] To model the falloff curves, values scaled with 0.55 (i.e., 82, 61, and 30 cm^{-1}) were used (see text).

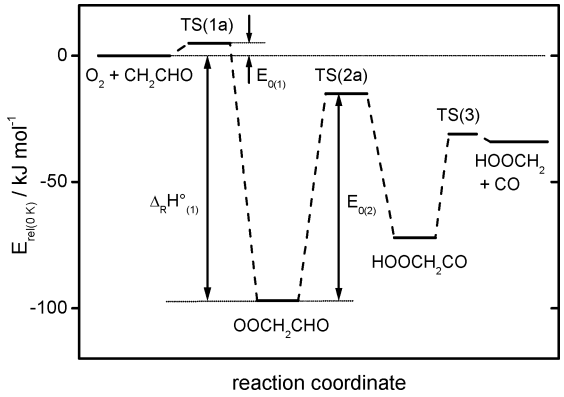

Figure 10. Potential energy diagram of reactions 1a−3 approximately to scale; $\Delta_R H°_{(1)}$, $E_{0(1)}$, and $E_{0(2)}$ are from experiment, all other data are from DFT calculations.[18]

unrealistic barriers $E_{0(1)}$ in the range 20−50 kJ mol^{-1}, which are in strong contradiction to the experimentally observed very weak temperature dependence of k_1. According to our calculations, TS(1a) is a very early transition state. The lengths of the O−O and the C═O bond vary less than 10% compared to the values in O_2 and CH_2CHO. We found that TS(1a) becomes less reactant-like in the following order of methods: B3LYP, QCISD, HF, MP2, each with the same basis set. A high spin contamination indicates that self-consistent field (SCF) and post-SCF methods cannot be expected to give a reliable relative energy. We conclude that the calculated barrier height for reaction 1a is the most uncertain thermochemical quantity in this reaction system. The structures of TS(2a) obtained at different levels of theory, however, are in good agreement with each other and exhibit features in line with similar reactions of other carbonyl-type radicals.[46]

We now employ our experimentally determined values for $\Delta_R H°_{0K(1)}$ and $E_{0(2)}$ to model the temperature and pressure dependence of k_1 using eqs 5−9. The weak temperature dependence of k_1 observed at high pressures can be reproduced by calculating $k_{1(\infty)}(T) = k_{1a(\infty)}(T)$ from simple canonical transition state theory[44] using the (unscaled) molecular and transition state data and assuming a very small barrier $E_{0(1)}$ around 1 kJ mol^{-1}. If eq 5 is solved with these parameters for low pressures, a ratio $k_{1(0)}/k_{1(\infty)} = 0.594$ is obtained for $T = 298$ K. With $k_{1(\infty)} \approx 3 \times 10^{-13}$ cm^3 s^{-1} from our experiments, it follows that $k_{1(0)} \approx 1.8 \times 10^{-13}$ cm^3 s^{-1}, which is clearly too high, as can be realized from Figure 6. Obviously, the forward reaction 2a is predicted to be too fast compared to the backward reaction −1a. If we assume that properties of the tight transition

TABLE 4: Calculated and Experimental Thermochemical Parameters for Reactions 1 and 2 for $T = 0$ K

$-\Delta_R H^\circ_{(1)}$ (kJ mol^{-1})	$E_{0(-1)}$ (kJ mol^{-1})	$E_{0(2)}$ (kJ mol^{-1})	method	ref
112.3	115.4		G2/RRKM	20
102.6[a]	115.1[a]	84.7[a]	CBSQ	17
		74.0[a]	B3LYP/6-31G(d)	17
78.2	88.3	85.4	B3LYP/6-31G(d, p)	18
95.8	115	81.6	CBS-QB3	18
76.1	110	109	MPW1K/6-31+G(d, p)	18
92.5	113	81.2	CBS-APNO	18
72.4	84.5	85.3	B3LYP/6-311G(d, p)//B3LYP/6-311G(d, p)	this work
74.0	89.3	84.7	B3LYP/6-311+G(3df,2p)//B3LYP/6-311G(d, p)	this work
92.5	120.3	96.7	QCISD(T)/6-311+G(3df,2p)//QCISD/6-311G(d, p)	this work
87.2	106.7	97.5	CCSD(T)/cc-pVTZ// QCISD/6-311G(d, p)	this work
70.0	120.1	94.1	CCSD(T)/cc-pVDZ// QCISD/6-311G(d, p)	this work
97 ± 4	98 ± 5[b]	82 ± 4	experiment (high pressure)	this work

[a] $T = 298$ K. [b] Based on $E_{0(1)} = 1 \pm 1$.

state TS(2a) are predicted more reliably than those of the loose transition state TS(1a) (see above), then it appears reasonable to increase the rate of reaction −1a by introducing additional looseness into TS(1a). It is unimportant how this is formally accomplished.[40,45] We scale the three lowest frequencies of TS(1a) by a common factor $\alpha < 1$ so as to fit the falloff data for all temperatures with one common value of ΔE_{SL}. Although these 2 parameters are correlated to some extent, they influence different features of the falloff curve. Whereas α mainly affects the ratio $k_{1(0)}/k_{1(\infty)}$, the parameter ΔE_{SL} shifts the falloff range of the s-shaped curve horizontally (decreasing α means decreasing $k_{1(0)}/k_{1(\infty)}$, and decreasing ΔE_{SL} shifts the falloff range toward higher pressures).

The curves for $\alpha = 0.55$ and $\Delta E_{SL} = 500$ cm^{-1} are displayed in Figure 6. The agreement with the experimental results over the whole temperature and pressure range is satisfactory. A comparison for different temperatures shows that the falloff curves intersect in a narrow range of bath gas densities near 10^{19} cm^{-3} (corresponding to pressures between 400 and 700 mbar for temperatures between 300 and 500 K), where nearly temperature-independent rate coefficients close to 2.5×10^{-13} cm^3 s^{-1} are predicted. Above this range, the temperature dependence is slightly positive; below this range, it is slightly negative. This is in agreement with the weak negative temperature dependence reported in the low-pressure studies by Gutman and Nelson[12] and Lorenz et al.[13]

The value assumed for ΔE_{SL} in our model seems somewhat high for He as the collider gas, but the fit becomes distinctively poorer for smaller values. We note that a better agreement for smaller values can only be achieved by decreasing the difference $E_{0(-1)} - E_{0(2)}$ and increasing $E_{0(-1)}$ at the same time. Some of the quantum chemical results in Table 4 point in this direction while others do not. In this case, a negative temperature dependence for ΔE_{SL} would also have to be introduced, which is physically questionable.[47]

Our model also predicts OH yields in reasonable accord with experimental results. Lorentz et al.[13] found a yield of 20% at 27 mbar; our model predicts 39%. Oguchi et al., in a preliminary report,[15,16] gave values between ~20% near 10 mbar and 10% near 270 mbar; our model predicts values between 58 and 7% for these pressures, respectively ($T = 298$ K). Obviously, the pressure dependence is somewhat overestimated, but if one considers the fact that the adjustment of the parameters was done with respect to k_1, the agreement appears satisfactory.

Despite the open questions, we believe that the above parameter set gives an adequate representation of $k_1(T,P)$ over the temperature and pressure range studied and even allows a limited extrapolation. Hence, we cast our falloff analysis in a more convenient parametrization, which can be used for kinetic modeling. A representation proposed by Fulle et al.[48] is adopted:

$$k_1(T,[\mathrm{M}]) = k_{\mathrm{rec}(0)}[\mathrm{M}]\left(\frac{1+y}{1+x}\right)F(x) + k_{1(0)}\left[1 - \frac{x}{1+x}F(x)\right] \quad (10)$$

with

$$x = k_{\mathrm{rec}(0)}[\mathrm{M}]/(k_{1(\infty)} - k_{1(0)}) \quad (11)$$

$$y = k_{1(0)}/(k_{1(\infty)} - k_{1(0)}) \quad (12)$$

and

$$\log[F(x)] = (\log F_{\mathrm{cent}})/[1 + \log^2 x] \quad (13)$$

The following parametrization was found to adequately fit our experimental data:

$$k_{1(0)} = 5.14 \times 10^{-14} \exp\left(\frac{210\ \mathrm{K}}{T}\right) \mathrm{cm}^3\ \mathrm{s}^{-1} \quad (14)$$

$$k_{1(\infty)} = 1.7 \times 10^{-12} \exp\left(-\frac{520\ \mathrm{K}}{T}\right) \mathrm{cm}^3\ \mathrm{s}^{-1} \quad (15)$$

$$k_{\mathrm{rec}(0)} = 1.0 \times 10^{-32} \exp\left(\frac{923\ \mathrm{K}}{T}\right) \mathrm{cm}^6\ \mathrm{s}^{-1} \quad (16)$$

$$F_{\mathrm{cent}} = \exp(-T/730\ \mathrm{K}) + \exp(-3000\ \mathrm{K}/T) \quad (17)$$

Here $k_{1(0)}$ and $k_{1(\infty)}$ are the low- and high-pressure limiting values of k_1, respectively, F_{cent} denotes the broadening factor,[45] and $k_{\mathrm{rec}(0)}$ accounts for adduct formation at low pressures. We emphasize, however, that $k_{\mathrm{rec}(0)}$ has no physical meaning outside this simple model. The quality of the resulting falloff curves is demonstrated in Figure 6. The agreement with the results from the master equation is excellent, and eqs 10−17 represent a reliable description of $k_1(T,P)$ at least for temperatures between 300 and 500 K and pressures between 1 mbar and 50 bar with an estimated error margin of ± 30%.

Summary

The kinetics of the $CH_2CHO + O_2$ reaction was experimentally studied over an extended temperature and pressure range. On the basis of quantum chemical calculations and statistical rate theory, the temperature and pressure dependence of the rate coefficient was rationalized and found to be in accord with a complex-forming mechanism. Thermochemical and kinetic

parameters were determined, and a readily applicable parametrization of the rate coefficient for kinetic modeling was given.

Acknowledgment. The authors thank the DAAD and EGIDE for travel funds within the PROCOPE program. The Laboratoire de Physicochimie des Processus de Combustion is "Unité Mixte de Recherche de l'Université de Lille 1 et du CNRS". The Centre d'Etudes et de Recherches Lasers et Applications (CERLA) is supported by the Ministère chargé de la Recherche, the Région Nord-Pas de Calais, and the Fonds Européen de Développement Economique des Régions. One of the authors (B.V.) is grateful for the Hungarian Scientific Research Fund (OTKA T046861 and F037648). We thank Claudia Kappler for help with the experiments and Dr. Frank Striebel for valuable discussions.

Supporting Information Available: Tables with detailed experimental conditions and rate coefficients k_1 (Tables IS and IIS) and equilibrium constants K_1 and rate coefficients k_2 (Tables IIS and IIIS). This material is available free of charge via the Internet at http://pubs.acs.org.

References and Notes

(1) Finlayson-Pitts, B. J.; Pitts, J. N., Jr. *Chemistry of the Upper and Lower Atmosphere*; Academic Press: San Diego, CA 2000.

(2) Gutbrod, R.; Schindler, R. N.; Kraka, E.; Cremer, D. *Chem. Phys. Lett.* **1996**, *252*, 221.

(3) Olzmann, M.; Kraka, E.; Cremer, D.; Gutbrod, R.; Andersson, S. *J. Phys. Chem. A* **1997**, *101*, 9421.

(4) Inoue, G.; Akimoto, H. *J. Chem. Phys.* **1981**, *74*, 425.

(5) Hunziker, H. E.; Kneppe, H.; Wendt, H. R. *J. Photochem.* **1981**, *17*, 377.

(6) Kleinermanns, K.; Luntz, A. C. *J. Phys. Chem.* **1981**, *85*, 1966.

(7) Dodd, J. A.; Hwang, E. S.; Castle, K. J.; DeBoer, G. D. *J. Phys. Chem. A* **2004**, *108*, 10965.

(8) Donaldson, D. J.; Okuda, I. V.; Sloan, J. J.; *Chem. Phys.* **1995**, *193*, 37.

(9) Schmidt, V.; Zhu, G. Y.; Becker, K. H.; Fink, E. H. *Ber. Bunsen-Ges. Phys. Chem.* **1985**, *89*, 321.

(10) Lissianski, V. V.; Zamansky, V. M.; Gardiner, W. C., Jr. In *Gas-Phase Combustion Chemistry*; Gardiner, W. C., Jr., Ed.; Springer: New York, 2000; p 1.

(11) Baulch, D. L.; Cobos, C. J.; Cox, R. A.; Frank, P.; Hayman, G.; Just, Th.; Kerr, J. A.; Murrells, T.; Pilling, M. J.; Troe, J.; Walker, R. W.; Warnatz, J. *Combust. Flame* **1994**, *98*, 59.

(12) Gutman, D.; Nelson, H. H. *J. Phys. Chem.* **1983**, *87*, 3902.

(13) Lorenz, K.; Rhäsa, D.; Zellner, R.; Fritz, B. *Ber. Bunsen-Ges. Phys. Chem.* **1985**, *89*, 341.

(14) Zhu, L.; Johnston, G. *J. Phys. Chem.* **1995**, *99*, 15114.

(15) Oguchi, T.; Sato, Y.; Matsui, H. Presented at the 18th International Symposium on Gas Kinetics, Bristol, UK, 2004; Poster B13.

(16) Oguchi, T. Toyohashi University of Technology, Japan. Private communication, 2005.

(17) Lee, J.; Bozzelli, J. W. *J. Phys. Chem. A* **2003**, *107*, 3778.

(18) Kuwata, K. T.; Templeton, K. L.; Hasson, A. S. *J. Phys. Chem. A* **2003**, *107*, 11525.

(19) Kuwata, K. T.; Hasson, A. S.; Dickinson, R. V.; Petersen, E. B.; Valin, L. C. *J. Phys. Chem. A* **2005**, *109*, 2514.

(20) Oguchi, T.; Miyoshi, A.; Koshi, M.; Matsui, H.; Washida, N. *J. Phys. Chem. A* **2001**, *105*, 378.

(21) Delbos, E.; Devolder, P.; El Maimouni, L.; Fittschen, C.; Brudnik, K.; Jodkowski, J. T.; Ratajczak, E. *Phys. Chem. Chem. Phys.* **2002**, *4*, 2941.

(22) Forster, R.; Frost, M.; Fulle, D.; Hamann, H. F.; Hippler, H.; Schlepegrell, A.; Troe, J. *J. Chem. Phys.* **1995**, *103*, 2949.

(23) Hippler, H.; Striebel, F.; Viskolcz, B. *Phys. Chem. Chem. Phys.* **2001**, *3*, 2450.

(24) Planckaert, A. A.; Doucet, J.; Sandorfy, C. *J. Chem. Phys.* **1974**, *60*, 4846.

(25) Møller, C.; Plesset, M. S. *Phys. Rev.* **1934**, *46*, 618.

(26) Hehre, W. J.; Radom, L.; Schleyer, P. v.R.; Pople, J. A. *Ab Initio Molecular Orbital Theory*; Wiley: New York, 1986.

(27) Pople, J. A.; Head-Gordon, M.; Raghavachari, K. *J. Chem. Phys.* **1987**, *87*, 5968.

(28) Čižek, J. *J. Chem. Phys.* **1966**, *45*, 4256.

(29) Purvis, G. D., III; Bartlett, R. J. *J. Chem. Phys.* **1982**, *76*, 1910.

(30) Parr, R. G.; Yang, W. *Density-Functional Theory of Atoms and Molecules*; Oxford University Press: Oxford, U.K., 1989.

(31) Becke, A. D. *J. Chem. Phys.* **1993**, *98*, 5648.

(32) Dunning, T. H., Jr. *J. Chem. Phys.* **1989**, *90*, 1007.

(33) Frisch, M. J.; Trucks, G. W.; Schlegel, H. B.; Scuseria, G. E.; Robb, M. A.; Cheeseman, J. R.; Zakrzewski, V. G.; Montgomery, J. A., Jr.; Stratmann, R. E.; Burant, J. C.; Dapprich, S.; Millam, J. M.; Daniels, A. D.; Kudin, K. N.; Strain, M. C.; Farkas, O.; Tomasi, J.; Barone, V.; Cossi, M.; Cammi, R.; Mennucci, B.; Pomelli, C.; Adamo, C.; Clifford, S.; Ochterski, J.; Petersson, G. A.; Ayala, P. Y.; Cui, Q.; Morokuma, K.; Malick, D. K.; Rabuck, A. D.; Raghavachari, K.; Foresman, J. B.; Cioslowski, J.; Ortiz, J. V.; Baboul, A. G.; Stefanov, B. B.; Liu, G.; Liashenko, A.; Piskorz, P.; Komaromi, I.; Gomperts, R.; Martin, R. L.; Fox, D. J.; Keith, T.; Al-Laham, M. A.; Peng, C. Y.; Nanayakkara, A.; Gonzalez, C.; Challacombe, M.; Gill, P. M. W.; Johnson, B.; Chen, W.; Wong, M. W.; Andres, J. L.; Gonzalez, C.; Head-Gordon, M.; Replogle, E. S.; Pople, J. A. *Gaussian 98*, revision A.7; Gaussian Inc.: Pittsburgh, PA, 1998.

(34) Troe, J. *J. Chem. Soc., Faraday Trans.* **1994**, *90*, 2303.

(35) Gilbert, R. G.; Smith, S. C. *Theory of Unimolecular and Recombination Reactions*; Blackwell: Oxford, U.K., 1990.

(36) Holbrook, K. A.; Pilling, M. J.; Robertson, S. H. *Unimolecular Reactions*, 2nd ed.; Wiley: Chichester, U.K., 1996.

(37) Marcus, R. A.; Rice, O. K. *J. Phys. Colloid Chem.* **1951**, *55*, 894; Marcus, R. A. *J. Chem. Phys.* **1952**, *20*, 359.

(38) Troe, J. *J. Chem. Phys.* **1983**, *79*, 6017.

(39) Beyer, T.; Swinehart, D. F. *Commun. ACM* **1973**, *16*, 379.

(40) Astholz, D. C.; Troe, J.; Wieters, W. *J. Chem. Phys.* **1979**, *70*, 5107.

(41) Press, W. H.; Flannery, B. P.; Teukolski, S. A.; Vetterling, W. T. *Numerical Recipes in Fortran*, 2nd ed.; Cambridge University Press: Cambridge, U.K., 1992.

(42) Olzmann, M. *Phys. Chem. Chem. Phys.* **2002**, *4*, 3614.

(43) Hippler, H.; Nasterlack, S.; Striebel, F. *Phys. Chem. Chem. Phys.* **2002**, *4*, 2959.

(44) Glasstone, S.; Laidler, K. J.; Eyring, H. *The Theory of Rate Processes*, McGraw-Hill: New York, 1941.

(45) Troe, J. *Ber. Bunsen-Ges. Phys. Chem.* **1983**, *87*, 161.

(46) Viskolcz, B.; Bérces, T. *Phys. Chem. Chem. Phys.* **2000**, *2*, 5430.

(47) Oref, I.; Tardy, D. C. *Chem. Rev.* **1990**, *90*, 1407.

(48) Fulle, D.; Hamann, H. F.; Hippler, H.; Troe, J. *J. Chem. Phys.* **1996**, *105*, 983.